AD A105225

OFFICE OF NAVAL RESEARCH

CONTRACT N00014-78-C-0584

Technical Report, No.

⑥ SOME ASPECTS OF ULTRASONIC NONSPECULAR REFLECTION

by

Walter G. Mayer and Tran D. K. Ngoc

DTIC
ELECTE
OCT . 1981
S   D
B

Walter G. Mayer
Principal Investigator
Department of Physics
Georgetown University
Washington, DC 20057

Oct 81

REPORT DOCUMENTATION PAGE	READ INSTRUCTIONS BEFORE COMPLETING FORM
1. REPORT NUMBER GUUS 10814 2. GOVT ACCESSION NO. AD-A105225	3. RECIPIENT'S CATALOG NUMBER
4. TITLE (and Subtitle) Some Aspects of Ultrasonic Nonspecular Reflection	5. TYPE OF REPORT & PERIOD COVERED Technical 15 Oct 80 - 30 Sep 81
	6. PERFORMING ORG. REPORT NUMBER TR 4
7. AUTHOR(s) Tran D. K. Ngoc and Walter G. Mayer	8. CONTRACT OR GRANT NUMBER(s) N00014-78-C-0584
9. PERFORMING ORGANIZATION NAME AND ADDRESS Physics Department Georgetown University Washington, DC 20057	10. PROGRAM ELEMENT, PROJECT, TASK AREA & WORK UNIT NUMBERS 121108
11. CONTROLLING OFFICE NAME AND ADDRESS Office of Naval Research, Code 421 Arlington, VA 22217	12. REPORT DATE 1 October 1981
	13. NUMBER OF PAGES 15
14. MONITORING AGENCY NAME & ADDRESS(if different from Controlling Office)	15. SECURITY CLASS. (of this report) Unclassified
	15a. DECLASSIFICATION/DOWNGRADING SCHEDULE

16. DISTRIBUTION STATEMENT (of this Report)

Approved for public release; distribution unlimited

17. DISTRIBUTION STATEMENT (of the abstract entered in Block 20, if different from Report)

Approved for public release; distribution unlimited

18. SUPPLEMENTARY NOTES

19. KEY WORDS (Continue on reverse side if necessary and identify by block number)

Ultrasonics, solid plate, nonspecular reflection and transmission, Rayleigh angle reflectivity, acousto-optic interaction

20. ABSTRACT (Continue on reverse side if necessary and identify by block number)

A general description is given of the ultrasonic nonspecular reflection and transmission effects for layered media. This description forms the basis for evaluation, via acoustooptic interaction techniques to measure reflectivity from solid plates in a liquid and also for the detection of local inhomogeneities of the plate.

This Technical Report describes work performed under Contract N00014-78-C-0584, "Linear and Nonlinear Ultrasonic Interactions on Liquid-Solid Boundaries". The Report consists of reprints of the following articles:

"Optical methods for measuring ultrasonic reflection from solid plates" by W. G. Mayer and T. D. K. Ngoc, Acoustics Letters 3, 171 (1980)

"A general description of ultrasonic nonspecular reflection and transmission effects for layered media" by T. D. K. Ngoc and W. G. Mayer, IEEE Trans. SU 27, 229 (1981)

"Detection of local inhomogeneities in solids by Rayleigh angle reflection" by W. G. Mayer, Ultrasonics 19, 109 (1981).

Experimants and calculations described in the first two papers were performed at Georgetown University. The method described in the third paper was developed under this Contract at Georgetown University but the experiments reported in the paper were conducted at the Universität des Saarlandes, Saarbrücken, Federal Republic of Germany, while the Principal Investigator spent his sabbatical leave at that institution, supported through an award by the Humboldt Foundation, Bonn.

<div align="right">
Walter G. Mayer
Principal Investigator
</div>

Washington, DC, October 1981

OPTICAL METHOD FOR MEASUREMENT OF ULTRASONIC REFLECTION FROM SOLID PLATES.

Walter G. Mayer and Tran D.K. Ngoc.

Department of Physics, Georgetown University, Washington, DC 20057, U.S.A.

Abstract

An acousto-optic interaction method was used to measure the modulus of the reflection for ultrasonic waves impinging at various angles on solid plates immersed in water. Theory and experiment are shown to agree qualitatively when the product frequency times plate thickness is small.

Introduction

The reflection coefficient of ultrasonic waves from a solid plate immersed in a liquid has been given by Pitts et al. [1] for the simplified case where absorption is neglected. The general form of this amplitude reflection coefficient

$$R_A = N/F_a F_s \tag{1}$$

is the same when absorption is included, as was done by Ngoc [2], in which case the quantities in eq. (1) are defined in the following manner.

$$N = N_1^2 + N_2^2 - N_3^2 + 2N_1 N_2 (1 - \cos P \cos Q)/(\sin P \sin Q), \tag{2}$$

$$F_a = [(1 - \cos P)/\sin P]\ N_1 + [(1 - \cos Q)/\sin Q]\ N_2 + iN_3, \tag{3}$$

$$F_s = [(1 + \cos P)/\sin P]\ N_1 + [(1 + \cos Q)/\sin Q]\ N_2 - iN_3, \tag{4}$$

$$N_1 = (k_s^2 - 2k_x^2)^2, \tag{5}$$

$$N_2 = 4k_x^2 K_d K_s, \tag{6}$$

$$N_3 = \rho k_s^4 K_d K, \tag{7}$$

with the symbols in eqs. (2)-(7) given by

$$
\left.
\begin{aligned}
k &= (2\pi f/v)(1 + ia/2\pi), \\
k_d &= (2\pi f/v_d)(1 + ia_d/2\pi), \\
k_s &= (2\pi f/v_s)(1 + ia_s/2\pi), \\
k_x &= k \sin\theta_i,
\end{aligned}
\right\} \tag{8}
$$

$$
\left.
\begin{aligned}
K &= (k^2 - k_x^2)^{1/2}, \\
K_d &= (k_d^2 - k_x^2)^{1/2}, \\
K_s &= (k_s^2 - k_x^2)^{1/2},
\end{aligned}
\right\} \tag{9}
$$

$$
\left.
\begin{aligned}
P &= dK_d, \\
Q &= dK_s.
\end{aligned}
\right\} \tag{10}
$$

Here d is the thickness of the solid plate (in mm) and f the ultrasonic frequency (in MHz). The angle of incidence is denoted by θ_i, and ρ is the ratio of the liquid density to the solid density. The parameters v, v_d, v_s, and a, a_d, a_s are the sound velocities and attenuation per wavelength of the wave in the liquid, and the longitudinal and shear waves in the solid, respectively.

Numerical evaluation of the reflection coefficient, eq. (1), shows that reflection peaks occur for some θ_i with the number of peaks generally increasing when the product fd increases. The height of these peaks and the minima of R_A between peaks depend strongly on the values of a_d and a_s. The reflectivity pattern is rather complicated when fd becomes larger than about 10, making the experimental measurement of R_a as a function of θ_i difficult due to the existence of non-specular reflection [3].

However, when thin plates are selected the results of calculations based on eq. (1) can be verified experimentally using an acousto-optic interaction technique. This method and the results are described below.
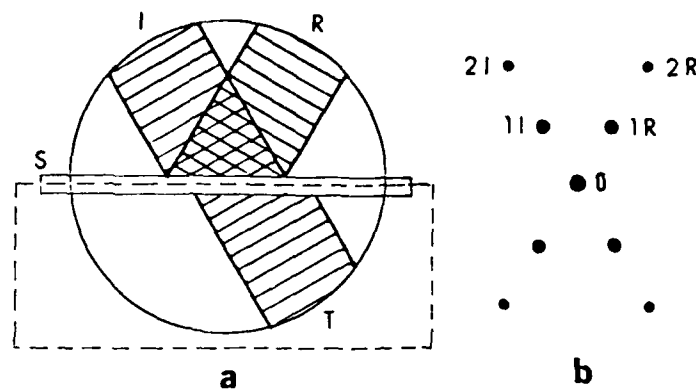
a   b

Figure 1   (a) Schematic diagram of beam alignment with respect to solid reflector (S). Incident, reflected, and transmitted beams are denoted by I, R, and T, respectively.
(b) Schematic diagram of alignment of first and second orders of diffraction patterns produced by incident and reflected ultrasonic beams shown in (a)

Method and Results

The experimental setup consists of a basic Raman-Nath [4] diffraction arrangement, part of which is shown schematically in Fig. 1a. A laser beam is expanded into a collimated beam of approximately 10 cm diameter, indicated by the circle in Fig. 1a. This beam travels through a glass tank filled with water, and the upper surface of the solid plate reflector (S) is located in the center of the beam. This surface is parallel to the propagation vector of the light so that an ultrasonic incident beam (I), the reflected beam (R) and the transmitted beam (T) are at right angles to the light propagation direction, satisfying the simplest conditions of light diffraction by ultrasonic waves as given by Raman and Nath [4];

A large lens (about 10 cm diameter) is used to focus the light beam after it has traversed the water in the glass tank. With no sound field present in the path of all the light will be focused in one point, indicated by 0 in Fig. 1b. However, if I, R, and T are present, diffraction patterns will be formed centered around 0. The alignment of the diffraction pattern caused by the incident beam, indicated by 2I, 1I, 0, etc. depends on the angle of incidence of the beam I, and the alignment of the pattern created by the reflected beam (2R, 1R, 0, etc) on the direction of travel of R. The transmitted beam T will produce a diffraction pattern which is superimposed on the pattern generated by I, since I and T have the same direction of travel. Thus, if one blocks all the light traversing the water below the solid plate, indicated by the dashed line in Fig. 1a, one obtains a set of diffraction patterns caused only by I and R.

The light intensity contained in the first orders of the diffraction pattern, i.e., I_{1I} or I_{1R}, depends on the amplitudes of the two ultrasonic beams I and R. Since the sound amplitude of the reflected beam changes as a function of the angle of incidence, as predicted from eq. (1), the light intensity I_{1R} also changes according to the theory of Raman and Nath. This light intensity is given by

$$I_{1R} = J_1^2(v_R) , \qquad (11)$$

where J_1 is the first-order Bessel function, whose argument v_R is proportional to the amplitude of the reflected ultrasonic beam.

If one now keeps v_I, the amplitude of the incident beam, constant as one changes the angle of incidence, one can compare the changing I_{1R} to the fixed I_{1I}. One can thus plot the amplitude of the reflected ultrasonic beam in comparison to the incident amplitude. This procedure yields a plot of reflectivity for a given solid reflector as a function of θ_i.
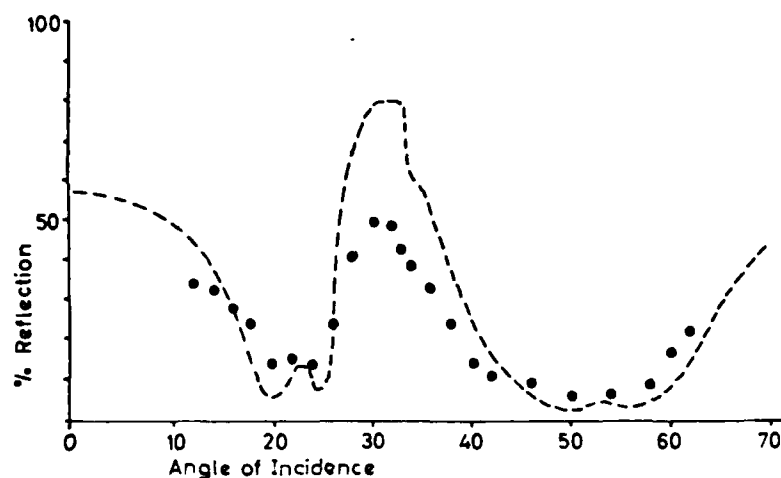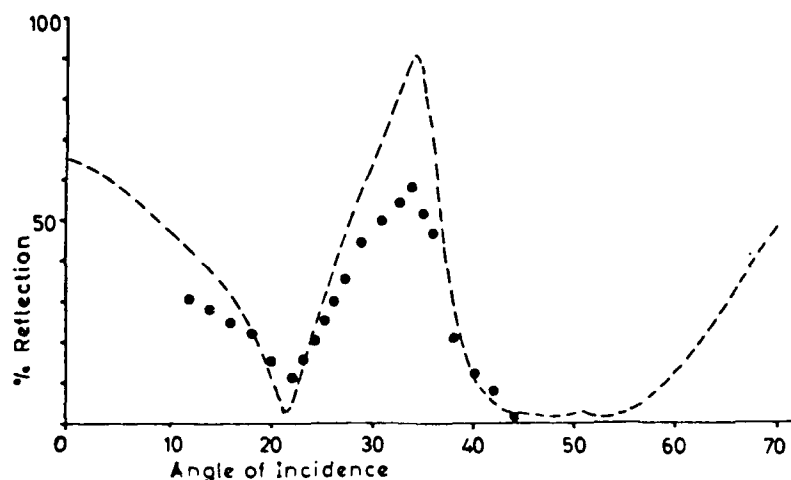
Figure 2   Calculated values (dashed line) and experimentally measured values
(circles) of reflection coefficient for a Plexiglas plate in water. Frequency 2 MHz, plate thickness 1/16 inch, fd = 3.175 MHz.mm

Figure 3   Calculated values (dashed line) and experimentally measured values
(circles) of reflection coefficient for a Plexiglas plate in water. Frequency 2 MHz, plate thickness 1 mm, fd = 2 MHz.mm

The results for two thin Plexiglass plates in water are shown in Figs 2 and 3.
The dashed lines are the theoretically calculated curves for the reflection coefficient
where the computation is based on eq. (1). Qualitative agreement exists, particularly referring to location and number of reflection maxima and minima. The
quantitative agreement is marginal, caused primarily by uncertainties about the
exact value of the absorption coefficient for both the longitudinal and shear wave
absorption coefficient of Plexiglas. An analysis of eq. (1) shows that the heights
of the reflection coefficient peaks and the depth of the minima are extremely
strong functions of the absorptivity, while the location and the number of extrema
are not materially influenced by the value of the absorptivity.

It should be noted that the method described here is applicable when the
reflected beam has an amplitude cross-section which is essentially the same as that
of the incident beam. This condition is satisfied in most cases where fd is small.
However, when fd becomes large, non-specular reflections and phase shifts between
portions of the reflected beam may occur [5], and the simple form of the uniform-beam Raman-Nath theory may no longer hold.

Conclusion

The acousto-optic interaction method described above can be used to determine the locations of reflection coefficient maxima and minima for ultrasonic beams impinging at various angles on solid plates. The method yields qualitative results of the changes in the amplitude reflection coefficient of plates in a liquid provided phase shifts within the reflected beam are not severe.

Acknowledgement

References

[1]   L.E. Pitts, T.J. Plona, W.G. Mayer. IEEE-Trans. Sonics & Ultrs. SU-24, 101, (1977).

[2]   T.D.K. Ngoc, Ph.D. Thesis. Physics Department, Georgetown University, Washington, DC, (1979).

[3]   M. Behravesh, L.E. Pitts, W.G. Mayer. Acoustics Letters, 1, 165, (1977).

[4]   C.V. Raman and N.S. Nath. Proc. Indian Acad. Sci. A2, 406, (1935).

[5]   W.G. Neubauer. J. Appl. Phys. 44, 48, (1973).

A General Description of Ultrasonic Nonspecular Reflection and Transmission Effects for Layered Media

TRAN D. K. NGOC AND WALTER G. MAYER

Abstract—A numerical integration method is used to calculate the intensity distribution in reflected and transmitted beams for liquid–solid–liquid layered media. It is shown that the formulation describes all nonspecular reflection and transmission phenomena for all angles of incidence, including critical angles. It is found that the existence of nonspecular phenomena not only depend on the angle of incidence and the product frequency times solid thickness but also on the product frequency times beamwidth. Various examples are given for reflection and transmission for incident angles corresponding to critical angles, plate-mode angles, and between-mode angles.

I. INTRODUCTION

GEOMETRICAL reflection or transmission of an ultrasonic bounded beam produces a beam with probably a lower intensity level than the incident beam but with the same intensity distribution profile. This is called specular reflectivity or transmittivity. Nonspecular reflection or transmission effects refer to phenomena where the reflected or transmitted beam has an intensity distribution profile different than that of the incident beam; this may include a lateral beam displacement, one or several minimum intensity areas, and a trailing sound field. Fig. 1 illustrates some typical profiles of a beam nonspecularly reflected from or transmitted through a layered system.

Bertoni and Tamir [1] successfully developed an analytical model to describe nonspecular reflectivity for a liquid–solid system at Rayleigh angle incidence. Later Bertoni and Hou [2] slightly modified this analysis to incorporate attenuation in the media. In the same analytical framework, Breazeale *et al.* [3] examined the reflected profile observed at large distances from the liquid–solid interface. Pitts *et al.* [4] extended Bertoni and Tamir's model to investigate the profile of a bounded beam reflected from a solid plate immersed in a liquid. The same approach was also used by Ng [5] to study the transmitted profile for the same layered system. Their calculated results are qualitatively consistent with experimental observations but only applicable when the resonant conditions prevail, that is, for Rayleigh angle incidence in the liquid–solid case and for plate-mode incidence in the liquid–solid–liquid case. The limitations of the Bertoni and Tamir's formulation also stem from the fact that the mathematical analysis becomes prohibitively involved as the system to be considered becomes more complicated.
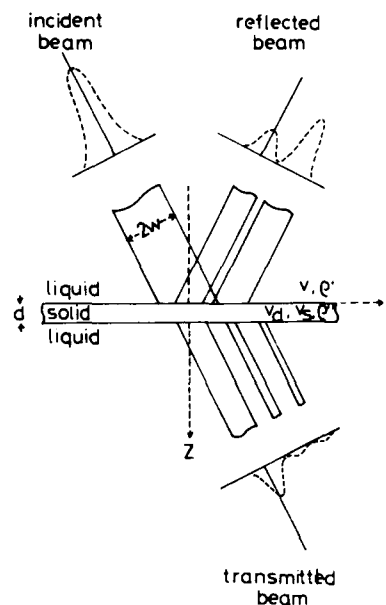
Fig. 1. Coordinate system and typical nonspecular profiles of reflected and transmitted beams.

Recently, another method which made use of numerical integration was developed by Ngoc [6] to describe nonspecular reflection phenomena for a liquid–solid system. This method was used to confirm the nonspecular reflection features for incidence near the Rayleigh critical angle and to establish nonspecular reflectivity for incidence near the longitudinal critical angle.

The present paper is intended to apply in general the numerical integration method to investigate the nonspecular reflection and transmission effects for a layered system. Results for incidence near critical angles of a liquid–solid system will be discussed, and nonspecular characteristics of a liquid–solid–liquid system will be investigated for both reflected and transmitted beams.

II. THEORETICAL FRAMEWORK

A. Spectral Representation of a Bounded Beam

Fig. 1 shows an incident ultrasonic beam bounded in the (x, z) plane and uniform in the y direction. The beam of angular frequency $\omega = 2\pi f$ is seen to be incident at an angle θ_i. Its intensity profile is contained by an effective width $2w$, which is projected onto the first interface as $2w_0$. The same

figure also illustrates the coordinate system for a liquid–solid–liquid structure. The same coordinate system is still useful for a liquid–solid system when the second interface is moved to infinity.

In the context of spectral analysis, a bounded beam can be represented as a superposition of an infinite number of plane waves which have different amplitude and wave vector. It is shown [7] by using Fourier analysis that the field of an incident beam can be uniquely determined at any point (x, z) if its field distribution is known in any plane. Thus a spectral representation of a well-defined incident beam can be expressed by the following Fourier integral transform pair

$$U_{\rm inc}(x, z) = (2\pi)^{-1} \int_{k_i - \pi/w_0}^{k_i + \pi/w_0} V(k_x) \exp\left[i(xk_x + zk_z)\right] dk_x$$

(1)

$$V(k_x) = \int_{-w_0}^{w_0} U_{\rm inc}(x, 0) \exp(-ixk_x)\, dx.$$

(2)

In (1) and (2), $U_{\rm inc}(x, 0)$ is the field distribution of the incident beam at the first interface where $z = 0$; k_x is the x component of the wave vector k; k_z is the z component of k defined by $k_z = (k^2 - k_x^2)^{1/2}$; the wave vector $k_i = (\omega/v)\sin\theta_i$ indicates the central direction of propagation of the incident waves; $V(k_x)$ is interpreted as the amplitude of the constituent plane waves. The time dependence, $\exp(-i\omega t)$, is suppressed. In this paper, the incident beam is taken to have a Gaussian distribution, and its sound field at the first interface is characterized by

$$U_{\rm inc}(x, 0) = \exp\left[-(x/w_0)^2 + ixk_x\right]$$

(3)

and hence from (2)

$$V(k_x) = \pi^{1/2} w_0 \exp\left[-(k_x - k_i)^2 (w_0/2)^2\right].$$

(4)

The physical interpretation of (1) is that the incident beam is composed of an infinite number of plane waves having the same wavelength but incident at different angles; in other words, the wave vector k_x is perturbed in a narrow range about k_i. The principle of spectral representation can be extended to describe a bounded beam reflected from or transmitted through layered media. If $P(k_x)$ denotes the plane wave reflection or transmission coefficients for a particular layered structure, then the associated sound field can be represented by

$$U(x, z) = (2\pi)^{-1} \int_{k_i - \pi/w_0}^{k_i + \pi/w_0} P(k_x)\, V(k_x)$$

$$\cdot \exp\left[i(xk_x + zk_z)\right] dk_x.$$

(5)

B. Plane Wave Reflection or Transmission Coefficients

It is evident from (5) that the relevant plane wave coefficient $P(k_x)$ strongly influences the beam profile. Indeed, (5) indicates that the resulting profile is constructed by the interference of the individual plane waves, which have amplitude $P(k_x) V(k_x)$ and undergo a phase shift upon reflection or

transmission. In this paper, one is interested in the profile of the sound beam reflected from a liquid–solid interface and those of both reflected and transmitted beams observed in the liquid–solid–liquid system.

The amplitude plane wave coefficients $P(k_x)$ for the cases of interest are given [8] by

$$R_{\rm LS}(k_x) = N/D$$

(6)

the reflection coefficient for a liquid–solid infinite half space system; and

$$R_{\rm LSL}(k_x) = N_R/F_a F_s$$

(7)

and

$$T_{\rm LSL}(k_x) = N_T/F_a F_s$$

(8)

for reflection and transmission for a liquid–solid–liquid system. The symbols used in (6)–(8) are defined as follows:

$$N = (k_s^2 - 2k_x^2)^2 + 4k_x^2 K_s K_d - \rho k_s^4 K_d/K$$

$$D = (k_s^2 - 2k_x^2)^2 + 4k_x^2 K_s K_d + \rho k_s^4 K_d/K$$

$$N_R = (k_s^2 - 2k_x^2)^4 + 16k_x^4 K_s^2 K_d^2 - \rho^2 k_s^8 K_d^2/K^2$$
$$\quad + 8(k_s^2 - 2k_x^2)^2 k_x^2 K_s K_d (1 - \cos P \cos Q)/(\sin P \sin Q)$$

$$N_T = (2i\rho k_s^4 K_d/K)\left[(k_s^2 - 2k_x^2)^2/\sin P + 4k_x^2 K_s K_d/\sin Q\right]$$

$$F_a = (k_s^2 - 2k_x^2)^2 (1 - \cos P)/\sin P$$
$$\quad + 4k_x^2 K_s K_d (1 - \cos Q)/\sin Q + i\rho k_s^4 K_d/K$$

$$F_s = (k_s^2 - 2k_x^2)^2 (1 + \cos P)/\sin P$$
$$\quad + 4k_x^2 K_s K_d (1 + \cos Q)/\sin Q - i\rho k_s^4 K_d/K$$

where

$$\rho = \rho'/\rho''$$
$$k = (\omega/v)(1 + ia/2\pi)$$
$$k_d = (\omega/v_d)(1 + ia_d/2\pi)$$
$$k_s = (\omega/v_s)(1 + ia_s/2\pi)$$
$$K = (k^2 - k_x^2)^{1/2}$$
$$K_d = (k_d^2 - k_x^2)^{1/2}$$
$$K_s = (k_s^2 - k_x^2)^{1/2}$$
$$P = dK_d$$
$$Q = dK_s.$$

The quantities a, a_d, and a_s denote the loss parameters defined as attenuation per wavelength for the sound waves in liquid and for the longitudinal and shear waves in solid, respectively.

It can be readily shown that $R_{\rm LS}(k_x)$ is a function of incident angle and frequency, while $R_{\rm LSL}(k_x)$ and $T_{\rm LSL}(k_x)$ are functions of incident angle and the product fd. The frequency dependence is present because the loss parameters depend on the sound frequency.

In general, the coefficients $P(k_x)$ are complex functions possessing pole-zero pairs which completely determine their analytical behavior in the complex plane [8]. These poles and zeros can be arranged into pairs because each consists of one pole and one zero, both having the same real part in the lossless case. For a liquid–solid–liquid system, the common real part of a pole-zero pair is associated with an angle of incidence
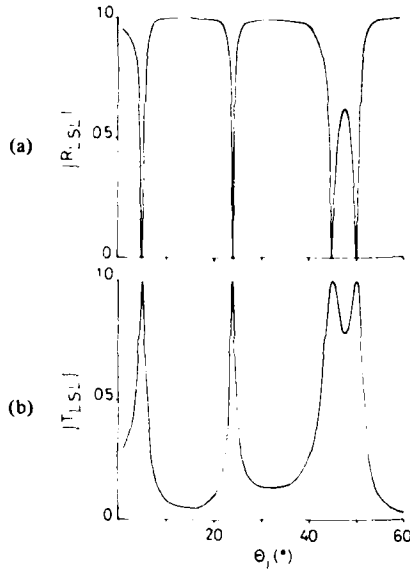
Fig. 2. Moduli for lossless water–brass–water system with fd = 2.4 km/s. (a) $R_{LSL}(k_x)$. (b) $T_{LSL}(k_x)$.
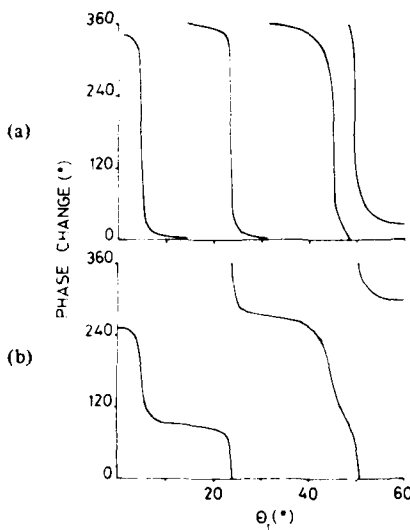

Fig. 3. Phases for lossless water–brass–water system with fd = 2.4 km/s. (a) $R_{LSL}(k_x)$. (b) $T_{LSL}(k_x)$.

where a plate mode can be excited. This association is expressed by the following relationship

$$|k_p|/|k| = |k_0|/|k| = \sin\theta_p \qquad (9)$$

where $|k| = \omega/v$, θ_p is the plate-mode angle of incidence, and k_p and k_0 are pole and zero of the same pair. At a plate-mode angle of incidence, $|R_{LSL}| = 0$ and $|T_{LSL}| = 1$ when the media are considered lossless, and the phase curves of R_{LSL} and T_{LSL} exhibit a point of inflection. Fig. 2 shows $|R_{LSL}|$ and $|T_{LSL}|$ as functions of incident angle for the lossless water–brass–water system with fd = 2.4 km/s. The relative phase of R_{LSL} and T_{LSL} for the same system is plotted versus angle of incidence in Fig. 3.
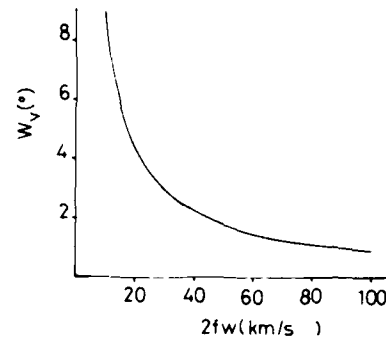

Fig. 4. Half-width W_v of $V(k_x)$ plotted against product frequency times beamwidth. Value used for θ_i is 30°.

C. Functional Characteristics of $V(k_x)$

Equation (5) also indicates that the resulting profiles are determined by the functional behavior of $V(k_x)$, which is the Fourier transform of the incident intensity distribution. It is seen from (4) that $V(k_x)$ is a Gaussian function whose shape depends on beamwidth, sound frequency, and angle of incidence. With the values of beamwidth being a few centimeters and those of frequency ranging from 1 MHz to 10 M ⌐⌐, the magnitude of $V(k_x)$ is significant only in a narrow range about k_i and almost independent of the values of incident angle. It is reasonable to represent the significant range of the Gaussian function $V(k_x)$ by its half-width. This half-width is denoted by W_v and can be written in units of degrees as

$$W_v = \sin^{-1}(\sin\theta_i + 0.53 W_k) - \sin^{-1}(\sin\theta_i - 0.53 W_k) \qquad (10)$$

where

$$W_k = v\cos\theta_i/2fw. \qquad (11)$$

Fig. 4 illustrates the functional dependence of W_v versus the product frequency times beamwidth for θ_i = 30°. Considering the known forms of $P(k_x)$ and $V(k_x)$, one can conclude that the calculated profile is a function of θ_i, f, and $2fw$ in the liquid–solid case, and of θ_i, fd, $2fw$ for a liquid–solid–liquid system.

D. Alternative Methods of Calculating Beam Profiles

To simplify the mathematical involvement and to avoid the complication that a beam profile may change as the beam travels away from the interfaces [3], the beam profiles for the cases of interest are all calculated at the interfaces, that is, at either $z = 0$ or $z = -d$. Under such circumstances, the sound field expressed by (5) becomes

$$U_{LS}(x, 0) = (2\pi)^{-1} \int_{k_i - \pi/w_0}^{k_i + \pi/w_0} R_{LS}(k_x) V(k_x)$$
$$\cdot \exp(ik_x x)\, dk_x \qquad (12)$$

$$U_{LSL}^R(x, 0) = (2\pi)^{-1} \int_{k_i - \pi/w_0}^{k_i + \pi/w_0} R_{LSL}(k_x) V(k_x)$$
$$\cdot \exp(ik_x x)\, dk_x \qquad (13)$$

$$U_{LSL}^{T}(x,-d) = (2\pi)^{-1} \int_{K_i - \pi/w_0}^{k_i + \pi/w_0} T_{LSL}(k_x) V(k_x)$$

$$\cdot \exp[i(k_x x - k_z d)] \, dk_x, \qquad (14)$$

where $U_{LS}(x,0)$ is the reflected field for a liquid-solid system, and $U_{LSL}^{R}(x,0)$ and $U_{LSL}^{T}(x,-d)$ are the reflected and transmitted fields for a liquid-solid-liquid system.

Two methods are known for the evaluation of (12)-(14). Bertoni and Tamir [1], Pitts [8], and Ng [5] chose to evaluate these integrals analytically after replacing the exact but complicated espressions of $P(k_x)$ with approximate ones constructed from the knowledge of the location of one or several pole-zero pairs they considered significant. This method will be referred to as the Bertoni and Tamir method. The other approach used by Ngoc [6] is to evaluate integrals numerically. The numerical integration method has been shown to be successful for some simple cases [9], [10].

The Bertoni and Tamir method essentially proceeds as follows: 1) determine the locations of pole-zero pairs of $P(k_x)$; 2) formulate a simple approximate expression for $P(k_x)$; and 3) carry out the still rather involved integration analytically. The numerical integration method proceeds in a more direct manner, numerically evaluating the integrals on the basis of the Simpson's integration algorithm thus omitting the mode-identifying step.

The numerical integration method is found to be efficient and adaptable to some practical considerations such as beam spreading effect and non-Gaussian incident profiles. In addition, the accuracy of the numerical integration method is not restricted to angles of incidence corresponding to resonant modes as is the case of the Bertoni and Tamir method. All calculated results presented below are obtained by the numerical integration method.

III. CALCULATED PROFILES FOR A LIQUID-SOLID SYSTEM

It has been established that for a liquid-solid system [6] nonspecular phenomena are prominent at such an angle of incidence that either or both of the modulus and phase of $R_{LS}(k_x)$ vary strongly. Such behavior is found near the longitudinal critical angle θ_d for a water-Plexiglas interface and near the Rayleigh critical angle θ_r for various liquid-solid interfaces. The reflected beam profile is a function of the absorption as well as of $\theta_i, f,$ and $2fw$. In the following calculations w and θ_i are varied, but f remains fixed. Therefore, profile changes as w is varied can be associated with $V(k_x)$, while changes resulting from variation of θ_i can be attributed to $R(k_x)$.

A. Incidence near Longitudinal Critical Angle

Fig. 5 shows the variation of the modulus and phase of $R_{LS}(k_x)$ near θ_d for a water-Plexiglas system at different frequency values. Both sets of curves exhibit strong variations in the angular range under consideration. Profiles of the reflected beam are calculated by the numerical integration
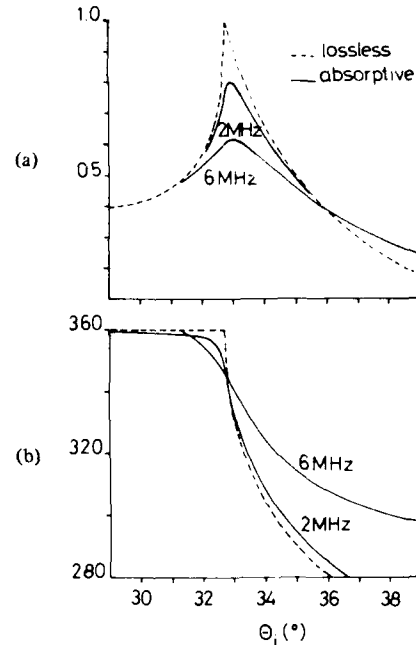

Fig. 5. Absorptive $R_{LS}(k_x)$ near longitudinal critical angle for water-Plexiglas interface. (a) Modulus. (b) Phase.
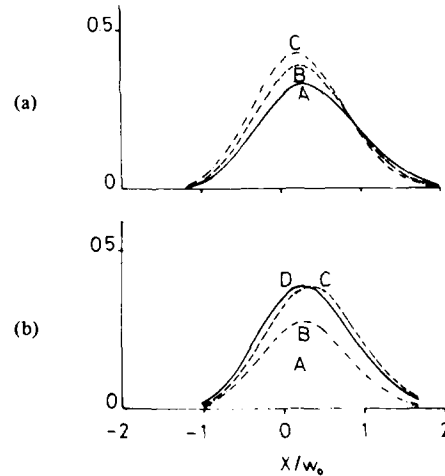

Fig. 6. Water-Plexiglas ($f = 2$ MHz): calculated reflected beam profiles. (a) $\theta_i = \theta_d$ as beamwidth is varied (A: 12.7 mm, B: 19.05 mm, and C: 25.4 mm). (b) Beamwidth is 19.05 mm as θ_i increases beyond θ_d (A: $\theta_d + 3°$, B: $\theta_d + 2$, C: $\theta_d + 1$, and D: θ_d).

method for $f = 2$ MHz when w and θ_i are changed. Nonspecular reflectivity is manifest only in the form of a lateral beam displacement, the magnitude of which varies significantly with both w and θ_i. These results are presented in Fig. 6. It is noted that the maximum beam displacement does not occur exactly at θ_d but approximately at $\theta_d + 1°$.

B. Incidence near Rayleigh Critical Angle

In Fig. 7, the modulus of $R(k_x)$ is plotted versus θ_i near θ_r for a water-stainless steel system. The phase curves are not
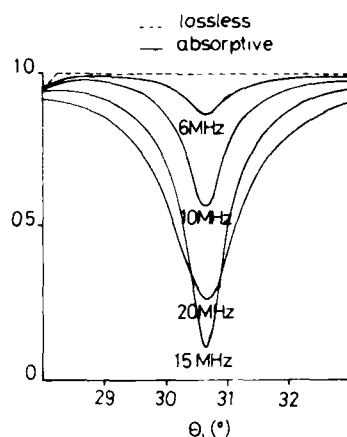
Fig. 7. Modulus of absorptive $R_{LS}(k_x)$ near the Rayleigh critical angle for water–stainless steel interface.
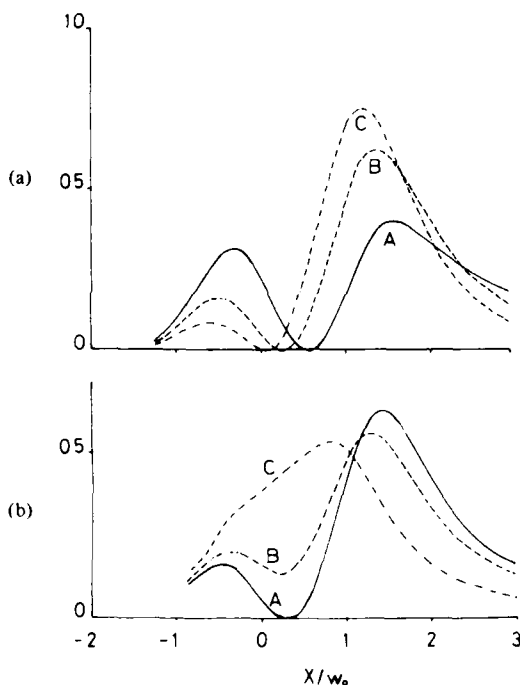

Fig. 8. Water–stainless steel ($f = 2$ MHz): calculated reflected beam profiles. (a) $\theta_i = \theta_r$ as beamwidth is varied (A: 12 mm, B: 20 mm, and C: 28 mm). (b) Beamwidth is 20 mm as θ_r is varied (A: θ_r, B: $\theta_r + 0.5°$, and C: $\theta_r + 1°$).

shown since they do not deviate significantly from the lossless case. Again the reflected beam profile is calculated for different values of w and θ_i, holding f fixed at 2 MHz. The non-specular characteristics consist of an intensity minimum, a beam displacement, and a trailing sound field. As the beamwidth becomes larger, the prominent change in the profile is a shift of the whole beam to the right. For variation of θ_i, the most noticeable profile change is seen at the intensity minimum which gradually gains in intensity and finally disappears approximately at $\theta_r + 1°$. These results are presented in Fig. 8.
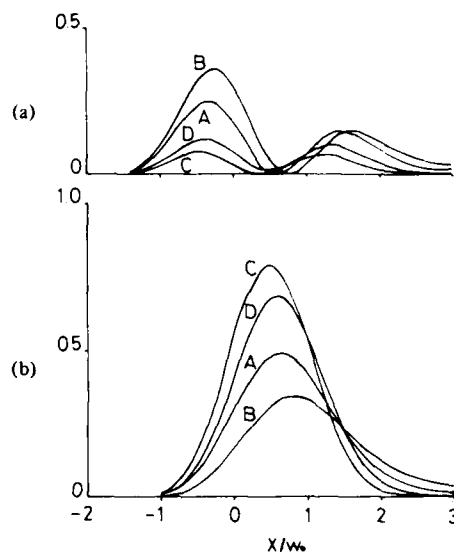

Fig. 9. Water–brass–water ($fd = 2.4$ km/s) beam profiles. (a) Reflected. (b) Transmitted. Calculated for $W_v = 2.4°$ at various plate-mode angles of incidence (A: $5°$, B: $24°$, C: $45°$, and D: $50°$).

IV. CALCULATED PROFILES FOR A LIQUID–SOLID–LIQUID SYSTEM

The numerical integration method is now applied to study a more complicated system of a solid plate immersed in a liquid. The integrals to be evaluated are (13) and (14), which describe the intensity profiles of the reflected and transmitted beams, respectively. As mentioned in Section II, the physical parameters of interest in this case are θ_i, f_d, and $2fw$. To separate the influence of $V(k_x)$ and $P(k_x)$, f is kept fixed at 2 MHz, and w and θ_i are varied.

It is interesting to investigate the profiles for different ranges of incident angles: those corresponding to plate modes and those falling between two adjacent modes. The former will be referred to as plate-mode incidence and the latter as between-mode incidence. For this reason, calculations for a water–brass–water system are done throughout for two values of fd, 2.4, and 7.0 km/s, since the plane wave coefficients exhibit different characteristics in terms of number of modes and spacings between modes for these values of fd. In the following, between-mode incidence is used to indicate the angle of incidence exactly between two adjacent plate modes, whose angular separation is denoted by S.

A. Plate-Mode Incidence

The profiles are first calculated at the plate-mode angles of incidence using $fd = 2.4$ km/s. The value of beamwidth is taken to be 19.05 mm, which gives $2fw = 38.1$ km/s. It is estimated from Fig. 4 that W_v is equal to 2.4°. Thus the beam profiles calculated with these parametric values would show only the functional behavior of $P(k_x)$ near a plate mode, because S is substantially larger than W_v (see Figs. 2 and 3). The reflected profiles plotted in Fig. 9 show features similar to those present in the beam reflected near θ_r from a liquid-solic
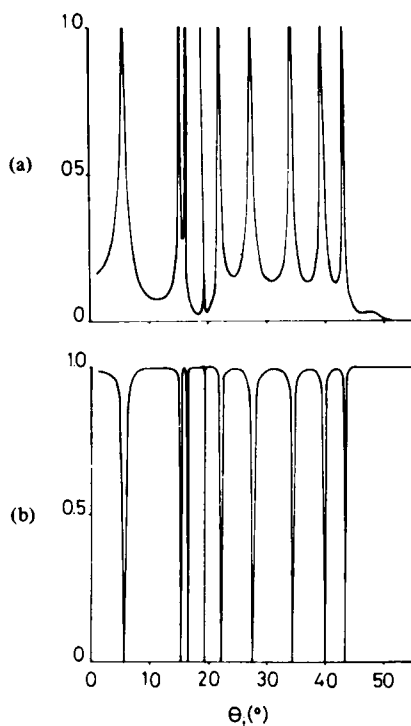
Fig. 10. Moduli for lossless water–brass–water system with $fd = 7.0$ km/s. (a) $T_{LSL}(k_x)$. (b) $R_{LSL}(k_x)$.

Fig. 11. Water–brass–water ($fd = 7.0$ km/s) beam profiles. (a) Reflected. (b) Transmitted. Calculated for $W_v = 2.4°$ at various between-mode angles of incidence (A: 15.6°, B: 24.7°, and C: 41.4°).

interface (compare Fig. 8). The same figure also shows the profiles calculated for the transmitted beam, displaying only a simple beam shift for all modes. The absence of an intensity minimum in the transmitted profiles can probably be attributed to the fact that the phase of $T_{LSL}(k_x)$ does not exhibit a 360° change as $R_{LSL}(k_x)$ normally does at plate-mode incidence. It is also noted that the intensity of the transmitted profiles increases with the width of the plate-mode peaks of the modulus curves.

B. Between-Mode Incidence

In this angular range $fd = 7.0$ km/s is used so that S varies noticeably for the same fd (Fig. 10). The chosen value of W_v is still 2.4°. Both reflected and transmitted profiles are calculated at three between-mode angles of incidence selected to be 15.6°, 24.7°, and 41.4°, whose values of S are 0.75°, 5.35°, and 3.6°, respectively. Fig. 11 shows the resultant profiles. It is observed that the profiles A display features characteristic of a plate-mode incidence profile, those labeled B have no noticeable nonspecular features, and the profiles C show an "interference" effect caused by the two adjacent modes. Comparison of the values of W_v and S leads to the following proposition: interference effect is most probable when $W_v < S < 2W_v$; nonspecular characteristics are not likely when $S > 2W_v$; and when $S \ll W_v$ a nonspecular profile produced in the neighborhood of two adjacent modes is similar to that resulting for plate-mode incidence.

C. Variation of Incident Angle

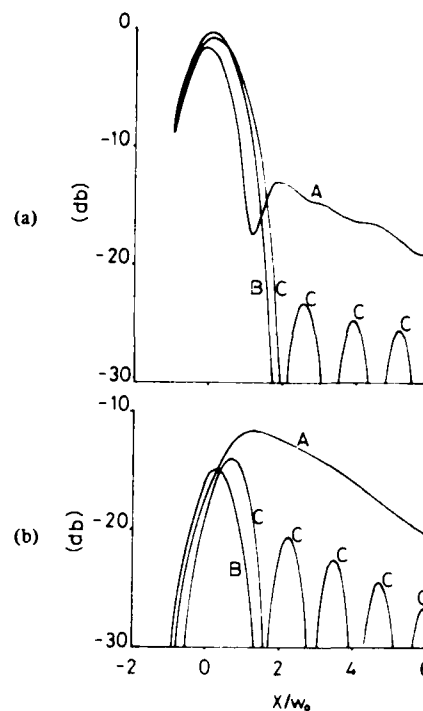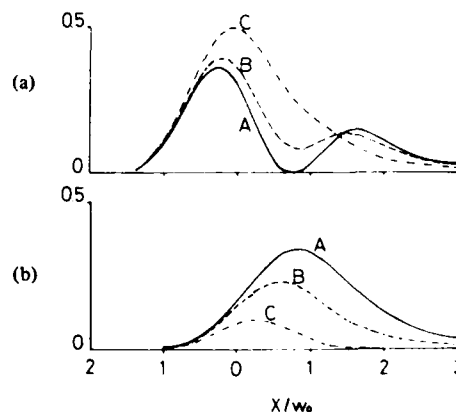The basic characteristics of the reflected and transmitted profiles have been established for plate-mode and between-

Fig. 12. Water–brass–water ($fd = 2.4$ km/s) beam profiles. (a) Reflected. (b) Transmitted. Calculated for $W_v = 2.4°$ and θ_i being varied about plate-mode incident angle $\theta_d = 24°$ (A: 24°, B: 25°, and C: 26°).

mode types of incidence. In this subsection, these are investigated to see how they change with the angle of incidence. Among those of Figs. 9 and 11, the profile for $\theta_i = 24°$ is chosen for the case of plate-mode incidence, and the one which exhibits the interference effect is chosen for investigation of the between-mode case. It is evident from Figs. 12 and 13 that, when θ_i is varied from its initial value, the nonspecular features become less pronounced and the nonspecular profiles are gradually transformed into specular ones. Fig. 13 in particular indicates that the interference peaks are less prominent as the incident angle deviates from the between-mode incidence of $\theta_i = 41.4°$.

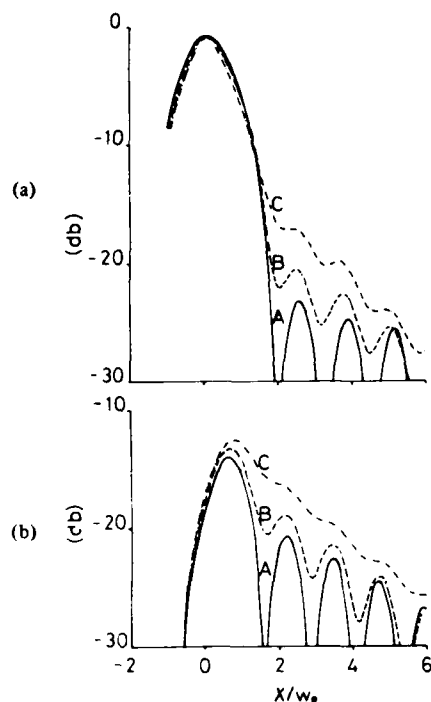Fig. 13. Water–brass–water (fd = 7.0 km/s) beam profiles. (a) Reflected. (b) Transmitted. Calculated for W_v = 2.4° and θ_i being varied about between-mode incident angle 41.4° (A: 41.4°, B: 41.1°, and C: 40.8°).

Fig. 15. Water–brass–water (fd = 7.0 km/s) beam profiles. (a) Reflected. (b) Transmitted. Calculated at between-mode incidence θ_i = 41.4° for various values of W_v (A: 2.4°, B: 3.55°, and C: 7.2°).
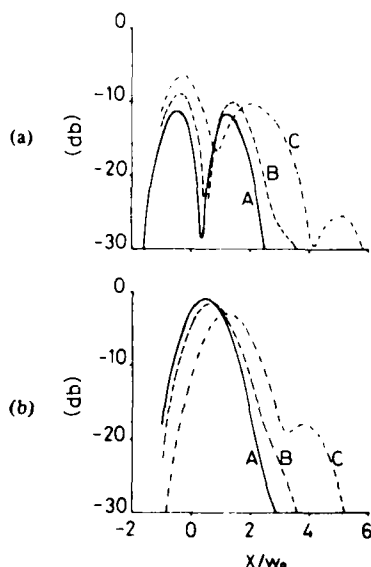

Fig. 14. Water–brass–water (fd = 2.4 km/s) beam profiles. (a) Reflected. (b) Transmitted. Calculated at plate-mode incidence θ_d = 45° for various values of W_v (A: 2.4°, B: 3.55°, and C: 7.2°).

D. Variation of Beamwidth

Finally, the profile changes are examined when the beamwidth is varied. Variation of the beamwidth amounts to a change in the half-width of $V(k_x)$. The beamwidth values used in the following calculations are 19.05 mm, 12.7 mm, and 6.35 mm. Therefore, the values of W_v derived from Fig. 4 are 2.4°, 3.55°, and 7.2°, respectively. Again calculations
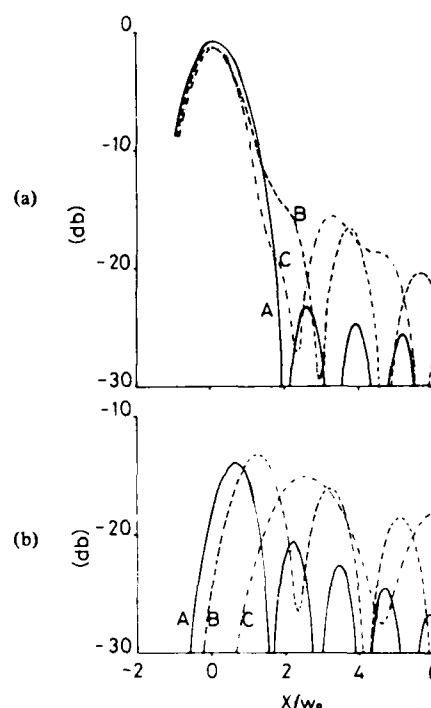
are done for both types of incidence, θ_i = 45° chosen for the plate-mode case and θ_i = 41.4° for the between-mode case. In the plate-mode case (Fig. 14), the profiles are qualitatively not changed when W_v is equal to 2.4° and 3.55°. For W_v = 7.2°, both reflected and transmitted profiles have an additional peak caused by the influence of the nearest mode (θ_i = 50°, i.e., 5° away), which is partially overlapping the mode under consideration. The results for between-mode incidence are illustrated in Fig. 15. The interference effect is still present for the low values of W_v. When W_v = 7.2°, both reflected and transmitted profiles show some plate-mode incidence character since the half-width W_v is now sufficiently larger than S which is equal to 3.6° in this case.

V. CONCLUSION

The numerical method described above, when applied to calculation of reflection from a liquid–solid interface, shows that nonspecular reflection of a Gaussian incident beam can occur at both the longitudinal and Rayleigh critical angles. The strength and observability of the effect depends on the frequency, the beamwidth, and the mechanical properties of the liquid–solid combination chosen.

The same method applied to a liquid–solid–liquid system yields information about nonspecular reflectivity and transmittivity. It is concluded from the results presented that θ_i and fd are not the only parameters of importance but that a new parameter, $2fw$, the product frequency times beamwidth, determines whether nonspecular reflection and transmission can be expected to occur at incident angles other than plate-mode angles of incidence.

REFERENCES

[1] H. L. Bertoni and T. Tamir, "Unified theory of Raleigh-angle phenomena for acoustic beams at liquid-solid interface," *Appl. Phys.*, vol. 2, pp. 157-172, 1973.

[2] H. L. Bertoni and Y. L. Hou, "Effects of damping in a solid on acoustic beams reflected at the Rayleigh critical angle," in *Proc. 10th Symp. NDE*, pp. 136-142, 1975.

[3] M. A. Breazeale, L. Adler, and G. W. Scott, "Interaction of ultrasonic waves incident at the Rayleigh angle onto a liquid-solid interface," *J. Appl. Phys.*, vol. 48, pp. 530-537, 1977.

[4] L. E. Pitts, T. J. Plona, and W. G. Mayer, "Theory of non-specular reflection effects for an ultrasonic beam incident on a solid plate in a liquid," *IEEE Trans. Sonics Ultrason.*, vol. SU-24, pp. 101-109, 1977.

[5] K. W. Ng, "Non-specular ultrasonic bounded beam transmission through solid plates," PhD. thesis, Physics Dep., Georgetown Univ., Washington, DC, 1979.

[6] T. D. K. Ngoc, "Influence of absorption on ultrasonic non-specular reflectivity," Ph.D. thesis, Physics Dep., Georgetown Univ., Washington, DC, 1979.

[7] L. M. Brekhovskikh, *Waves in Layered Media.* New York: Academic, 1960.

[8] L. E. Pitts, "A unified theoretical description of ultrasonic beam reflections from a solid plate in a liquid," Ph.D. thesis, Physics Dep., Georgetown Univ., Washington, DC, 1975.

[9] T. D. K. Ngoc and W. G. Mayer, "Ultrasonic non-specular reflectivity near longitudinal critical angle," *J. Appl. Phys.*, vol. 50, pp. 7948-7951, 1979.

[10] ——, "Numerical integration method for reflected beam profiles near Rayleigh angle," *J. Acoust. Soc. Amer.*, vol. 67, pp. 1149-1152, 1980.

Detection of local inhomogeneities in solids by Rayleigh angle reflection

W.G. MAYER

A schlieren method is employed to observe changes in the reflection profile of an ultrasonic beam incident at the Rayleigh angle. These changes are used to determine the location of small elastic inhomogeneities of a flat solid sample.

Introduction

Ultrasonic methods have been used for many years to determine not only the elastic properties of solids but also changes of these properties and inhomogeneities which influence propagation velocities in the solid. As early as 1946, Firestone and Frederick[1] used ultrasonic velocity measurements to find anisotropies in rolled aluminium. Changes in ultrasonic velocities can be caused by a variety of anisotropies, among them changes in Young's modulus[2] which may be measurable as variations in the shear wave velocity.[3] Longitudinal wave velocity changes can be caused by preferred orientations, as for instance in a drawn zinc bar where the velocity was found to vary[4] between 3540 m s^{-1} and 4400 m s^{-1}.

In addition to bulk wave velocity measurements one can use surface waves to determine changes in bulk properties[5] or texture.[6] Lamb waves can also be used[7] for the determination of irregularities in thin extended solids.

Generally, measurements made using these techniques reveal changes in sound velocities caused by anisotropies that exist either throughout the entire length of the sound path or within a portion of the measurement distance. However, a small isolated irregularity may contribute very little to the overall change in velocity determined over a relatively long distance which includes the irregularity. The method described below samples elastic properties of the solid and reveals small local changes in the ultrasonic velocity which, if a long path were used, could easily escape detection.

Theoretical background

The method described is based on the fact that a bounded ultrasonic beam incident from a liquid on to a flat solid may be non-specularly reflected if the angle of incidence is equal to the Rayleigh angle. One of these non-specular reflection phenomena, a lateral beam displacement, was first observed by Schoch.[8] Whether the reflected beam is laterally displaced or whether an intensity profile change occurs, that is, the reflected beam appears to split into two distinct portions separated by an intensity null region,[9] depends strongly on the beam width, the frequency, and

The author is presently at the Labor Kurzzeitphysik, Universität des Saarlandes, 6600 Saarbrücken, West Germany. His permanent address is the Physics Department, Georgetown University, Washington, DC 20057, USA, Paper received 28 November 1980.

on how closely the incidence angle approaches the Rayleigh angle.[10]

These changes in the reflected beam profile can be calculated if one considers the reflection coefficient for a bounded beam rather than a single plane wave. Representing[11] the incident beam as a summation of an infinite number of plane waves, all of the same frequency but incident at the boundary at different angles, one can construct the reflected sound field at the boundary for any point along the interface, that is, the x-direction. The amplitude distribution of the reflected beam is given[12] by

$$U_R(x) = (1/2\pi) \int_{-\infty}^{\infty} R(k_x)\, V(k_x) \exp(ixk_x)\, dk_x \qquad (1)$$

where $R(k_x)$ is the plane wave amplitude reflection coefficient, k_x is the projection of the incident wave vector on the x-axis, and $V(k_x)$, the Fourier transform of the incident particle displacement, depends on the incident field profile, $U_{inc}(x)$,

$$V(k_x) = \int_{-\infty}^{\infty} U_{inc}(x) \exp(-ixk_x)\, dx. \qquad (2)$$

Introducing attenuation, the various terms in the above expressions can be transformed in such a fashion that the reflected beam profile can be calculated by numerical integration.[13] Numerical evaluations for different flat solids immersed in water show that a Gaussian beam incident at the Rayleigh angle is reflected with an intensity profile that is quite different from a Gaussian distribution. The resulting profile depends on beam width and frequency and, most important for the present purpose, on whether the incidence is exactly at the Rayleigh angle or at a slightly different angle. This latter dependence is illustrated for the case of a water-stainless steel boundary as shown in Fig. 1, which is adapted from Ngoc.[10] The centre of the incident Gaussian beam, not shown in Fig. 1, is incident at point 0 on the x-axis. The graph indicates that the reflected beam profile is no longer Gaussian and changes markedly when the angle of incidence is changed slightly from θ_R, the Rayleigh angle.
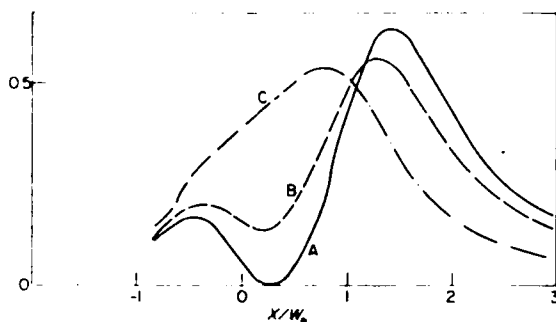
Fig. 1 Calculated profile of reflected beam at a water-stainless steel boundary for incident angles of: A, θ_R; B, $\theta_R + 0.5°$; C, $\theta_R + 1°$. Beam width is 20 mm, frequency 2 MHz, and incident beam (not shown) is centred at $X/W_o = 0$, where W_o is a measure of beam width. (After Ngoc[10])

Experimental method and results

The curves in Fig. 1 are given as a function of θ_i, the angle of incidence, for $\theta_i = \theta_R$ to $\theta_i = \theta_R + 1°$. The Rayleigh angle for stainless steel is 30.6°, determined by the Rayleigh wave velocity, v_R, and the sound velocity in water, v, according to

$$\sin \theta_i / v = 1/v_R. \qquad (3)$$

With $v = 1490$ m s^{-1} and $\theta_i = 30.6°$ one obtains $v_R = 2930$ m s^{-1}.

If one immerses a flat sample of stainless steel in water, a 2 MHz, 20 mm wide, Gaussian ultrasonic beam impinging at $\theta_i = \theta_R$ will be reflected according to curve A in Fig. 1. Such a profile can be observed visually with a standard Schlieren arrangement. If one now moves the sample parallel to its surface the profile will not change if v_R remains the same at all locations subjected to the incident beam. If, however, the beam profile observed at some location deviates from the previously observed shape, the value of v_R in (3) must be different at that particular location since neither θ_i nor v have changed.

One can easily observe on a homogeneous sample changes in the reflection profile caused by a change in the angle of incidence, $\Delta\theta_i$, of 0.25° (see Fig. 1) if one were to change the angle of incidence without moving the sample. Conversely, one can also notice quite readily changes in the profile caused by a change in the Rayleigh wave velocity, Δv_R, if one does not change θ_i but moves the sample, provided the sample is locally inhomogeneous. An example of this situation is shown in Fig. 2. Here a 10 mm wide, 2 MHz beam impinges on a flat (to at least 0.05°) thick brass sample. The angle of incidence is the Rayleigh angle and the resulting reflection profile is shown in Fig. 2a. Moving the sample parallel to its surface does not change the appearance of the reflected beam profile until one reaches an area on the sample where the elastic properties of the sample change, giving rise to a different non-specular reflection profile, shown in Fig. 2b. The original appearance can be restored by a slight adjustment of θ_i. In the case of this particular sample a decrease of 0.75° in θ_i was required.

Substituting this adjusted angle, $\theta_i = \theta_R - 0.75°$, into (3) and comparing the resulting value of v_R with that one obtains for the rest of the sample one finds that the local
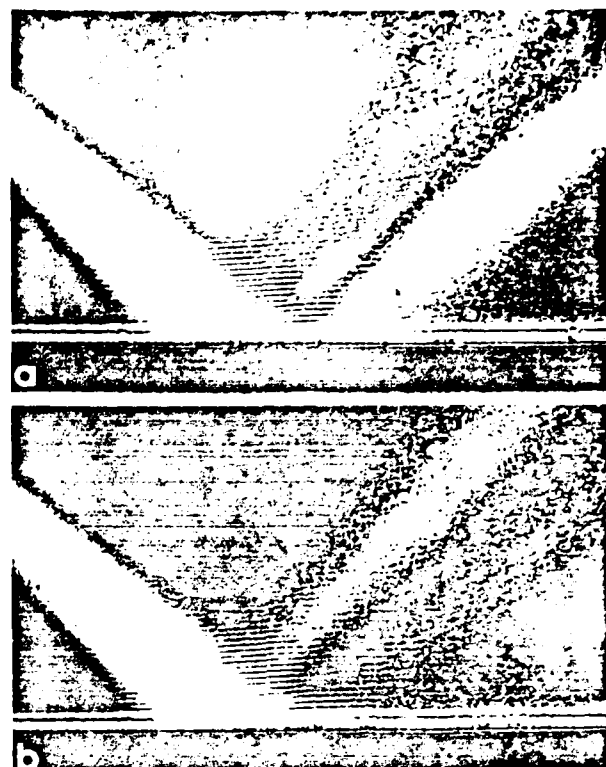

Fig. 2 Schlieren photographs of 2 MHz beam reflected at a brass-water flat interface with: a – Rayleigh angle incidence; and b – same angle of incidence but at section of sample with slightly different elastic properties

value of v_R is about 24 m s^{-1} higher than elsewhere on the sample. Thus, this method is sensitive to small, localized changes in the Rayleigh wave velocity.

Discussion

The method described above can be used to find local Rayleigh wave velocity fluctuations that can be as small as a fraction of one percent of v_R. Assuming that a profile change is detectable that corresponds to a 0.25° deviation from θ_R, the resulting detectability of a change in v_R depends on the magnitude of the unperturbed Rayleigh wave velocity. Fig. 3 shows the amount of Δv_R for $\Delta\theta_i$ of 0.25°, 0.5°, and 1° as a function of the overall v_R and the corresponding θ_R. The curves shown are for a solid-water boundary, calculated from (3) for positive $\Delta\theta_i$. The corresponding Δv_R for negative $\Delta\theta_i$ are shown as points.

Although this method enables one to detect small, local changes in the elastic properties one should not expect to be able also to determine the cause of these velocity anisotropies. Considering that v_R depends on the value of the shear wave velocity and on Poisson's ratio, which itself depends on the shear wave and the longitudinal wave velocities, any observed Δv_R may be caused by local fluctuations in these quantities. Moreover, since these bulk wave velocities depend on the elastic moduli and the density of the solid, an observed Δv_R may also be caused by anisotropies of these latter parameters.

Thus the method described here can be primarily useful in the location of small localized inhomogeneities of the solid while the determination of the exact causes can then be attempted with the appropriate techniques applied at the location in question.
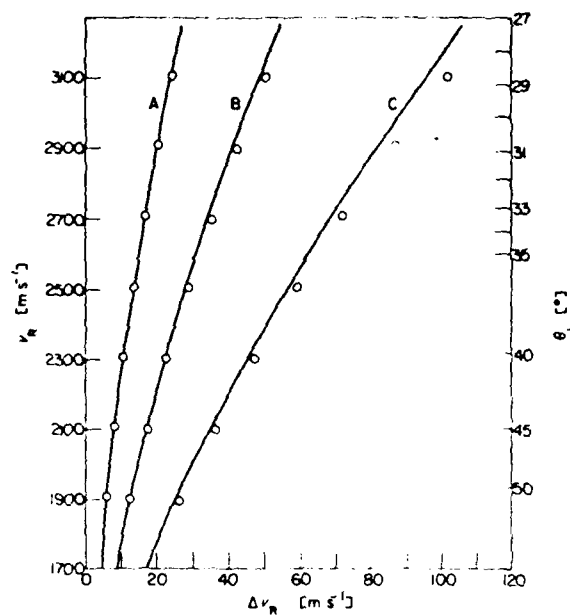
Fig. 3 Changes in v_R detectable with $\Delta\theta_i$ of: A, 0.25°; B, 0.5°; C, 1° as a function of v_R or θ_R

Acknowledgement

References

1   Firestone, F.A., Frederick, J.R., *J. Acoust. Soc. Am.* 18 (1946) 200
2   Alers, G.A., Liu, Y.C., *Trans AIME* 236 (1966) 482
3   Papadakis, E.P., Ch. 15 in Physical Acoustics IVB, W.P. Mason, ed., Academic Press (1968)
4   Papadakis, E.P., *J. Appl. Phys.* 36 (1965) 1738
5   Tittmann, B.R., Alers, G.A., Graham, L.J., *Metall. Trans.* 7A (1976) 229
6   Frederick, S.F., *Materials Eval.* (Sept. 1975) 213
7   Höller, P., Lechky, E., *Arch. Eisenhüttenw.* 33 (1962) 699
8   Schoch, A., *Acustica* 2 (1952) 1
9   Neubauer, W.G., *J. Appl. Phys.* 44 (1973) 48
10 Ngoc, T.D.K., Mayer, W.G., *J. Acoust. Soc. Am.* 67 (1980) 1149
11 Bertoni, H.L., Tamir, T., *Appl. Phys.* 2 (1973) 157
12 Pitts, L.E., Plona, T.J., Mayer, W.G., *IEEE Trans Sonics Ultras.* 24 (1977) 101
13 Ngoc, T.D.K., Mayer, W.G. *IEEE Trans Sonics Ultras.* 27 (1980) 229